2

An activatable, polarity dependent, dual-luminescent imaging agent with long luminescence lifetime

Abstract

Activatable luminescent imaging agents have the potential to generate highly sensitive and specific diagnostic read-outs. Examples where the concept is coupled to (long) lifetime imaging are few. In this study, an activatable imaging agent specifically designed for luminescence lifetime imaging is reported. When the two luminophores Cy5 and $Ir(ppy)_3$ were covalently linked, both emissions were quenched; Ir(ppy)3 is quenched by energy transfer to Cy5, and Cy5 is quenched by spin-orbit coupling induced by the iridium atom. Cleavage of the connective disulfide bond, either in solution or ***in vitro*** resulted in a >100-fold increase in the luminescence intensity for both luminophores. Activation also led to an increase in the luminescence lifetime of $Ir(ppy)_3$, going up to 90 ns. The availability of imaging agents with an activatable shift in lifetime, in our view, opens unique new opportunities in the field of lifetime imaging.

2.1. Introduction

Luminescence imaging is widely used in molecular cell biology and the technology is more and more explored in the clinical setting *e.g.* for surgical guidance.[1] While the emission of luminophores can be used directly, the (photo)physical interactions between different luminescent compounds also has value in diagnostic applications.[2] Uniquely, disturbance of the interaction between a luminophore and a quencher, or chemical modification of a luminophore, can generate disease-specific signals.[3, 4] Generally an activatable approach provides a measure for enzymatic activity.[5-7]

Organic dyes, which are most commonly explored as activatable imaging agents, are prone to interference from autofluorescence. This disturbance can be minimized by tailoring the wavelengths towards the far-red and near-infrared window where the autofluorescence is minimal.[8] Alternatively, luminophores may be designed to have a large Stokes shift (> 100 nm) to obtain a peak intensity that lies beyond the spectral range where autofluorescence generally occurs.[1] Luminescence lifetime may also help to separate exogenous from endogenous signals.[9]

We reasoned that the specificity of an activatable imaging agent can be improved by exploiting luminescence lifetimes that exceed those of endogenous molecules (0.1-7 ns).[10] Added advantages of phosphorescent transition complexes are their high photostability, large Stokes shift, and inability of self-quenching.[11] Previously some efforts have been made to use ruthenium or iridium complexes for imaging,[8, 12-16] and a few ruthenium complexes have been investigated that give a change in luminescence lifetime (τ > 10 ns).[17, 18] Iridium complexes allow two types of quenching: First, Förster Resonance Energy Transfer (FRET) or triplet-triplet energy transfer from an iridium complex to an organic moiety, thereby quenching the iridium-based phosphorescence.[19-21] Second, iridium atoms can induce spin-orbit coupling on other luminophores, quenching the other dye.[20, 21] In contrast to effective distances in FRET (up to 10 nm),[22] distances in spin-orbit coupling effects are confined to 1 nm.[23] Although spin-orbit coupling is considered a drawback in the efficiency of LEDs containing transition metals,[24] we aim to exploit this effect, in combination with FRET, as basis to generate a new class of activatable imaging agents.

The combination of luminescence signal activation and luminescence lifetime imaging was examined using an $Ir(ppy)_3$ complex and a Cy5 dye to combine the desired effects of both imaging strategies in a dual-luminescent imaging agent.

2.2. Results and discussion

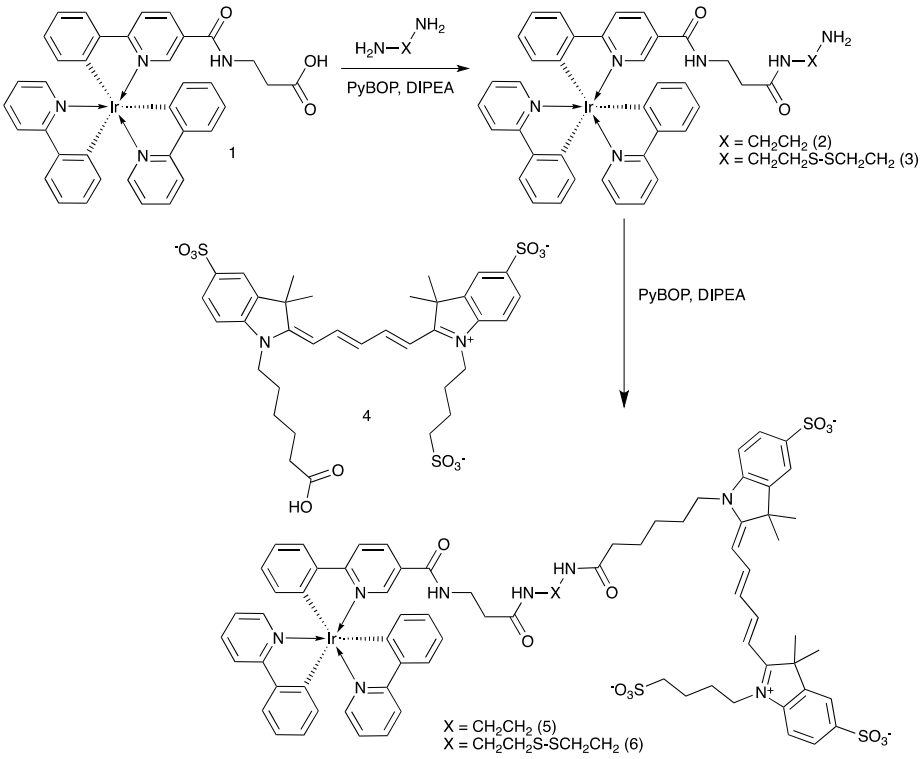

Scheme 1: Synthesis of $Ir(ppy)_3$-Cy5 compounds with different linkers

After synthesis of the $Ir(ppy)_3$-complex (**1**), a suitable linker was attached (**2-3**). Excess linker was used to minimize dimer formation (Scheme 1, see Appendix I (AI) for detailed experimental section). This resulted in yields of 42% (**2**) and 56% (**3**). Cy5 was chosen as FRET acceptor

because of its spectral overlap with $Ir(ppy)_3$ (Figure 1A) and high extinction coefficient ($\varepsilon = 2.5*10^5$). Compounds **5** and **6** were made to provide both stable and activatable derivatives of the conjugate. Conjugation with Cy5 (**4**) was achieved using standard peptide coupling chemistry. After purification, in both cases a blue/green solid was obtained in yields of 64 % (**5**) and 33 % (**6**).

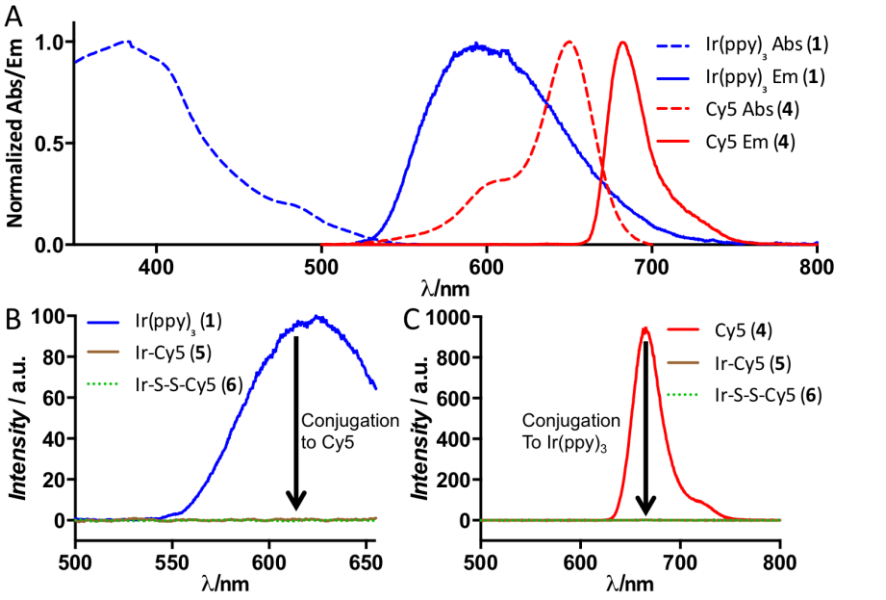

Figure 1: A) Normalized absorption and emission spectra of $Ir(ppy)_3$ and Cy5 in PBS showing the spectral overlap. B) Emission of equimolar solutions of 1, 5 and 6 with 457 nm excitation and C) emission of equimolar solutions of 4, 5 and 6 with 627 nm excitation in PBS

When $Ir(ppy)_3$ (**1**) is excited, it undergoes rapid inter-system crossing to a triplet excited state and from there emits phosphorescence light ($\varepsilon = 9*10^3$; $\Phi = 0.12$ (DMSO)).[25] FRET from $Ir(ppy)_3$ to Cy5 prevented $Ir(ppy)_3$ emission in **5** and **6** in phosphate buffered saline (PBS) (Figure 1B). Independent of the solvent, the $Ir(ppy)_3$ emission remained fully quenched indicating energy transfer occurs from $Ir(ppy)_3$ to the Cy5 singlet excited

state by FRET; we calculated the Förster distance between these luminophores to be 4.8 nm (see AI.2.).[26] The donor-acceptor distances in our compounds fall well within this distance, allowing for efficient quenching.

The spin-orbit coupling induced by the iridium atom was used to quench emission of Cy5 efficiently (Figure 1C) by allowing energy transfer from the singlet excited state of Cy5 to a non-emissive triplet excited state of Cy5 (Figure S1). Regardless the excitation wavelength (405 or 633 nm), at 77 K the emission spectra of **5** showed two peaks at 760 and 840 nm (Figure S3). These peaks correspond to the previously reported triplet state emission of Cy5.[27] Since in **5** and **6** the emission of both luminophores is substantially quenched (>99.7 %), we state that in PBS the luminescence is in the off-state when the luminophores are conjugated.

The difference in distance dependence between the two quenching mechanisms was used to largely mitigate spin-orbit coupling, while leaving FRET intact. Using MeOH as co-solvent increased the solvation of **5** and **6** and this resulted in Cy5 singlet emission at 670 nm upon excitation of $Ir(ppy)_3$ (Figure AI.2). In the absorption spectra, changing to a more apolar solvent leads to a decrease in the peak (610 nm) that indicates stacking interactions (Figure AI.4B). This conformational change resulted in a 30-fold increase of Cy5 fluorescence intensity (Figure AI.4C), while the $Ir(ppy)_3$ emission remained quenched. The rotational freedom of the molecules, however, seems to prevent complete signal restoration. The triplet emission caused by spin-orbit coupling in **5** (observed at 77 K in H_2O) disappeared upon reduction in polarity, also indicating a change in the interaction between Cy5 and the Ir atom (Figure AI.3A). Lastly ROESY

spectra in CD_3OD did not reveal close distance correlations between Cy5 and $Ir(ppy)_3$ (See AI.6).

Similar to the use of MeOH, micelles of SDS were able to increase the Cy5 luminescence intensity, providing a model system for interactions with the cell membrane. Only above the critical micelle concentration of 1 mM[28] an increase of Cy5 fluorescence intensity was observed (Figure AI.5). In line with these findings, interaction of **5** (the uncleavable derivative; Figure 2) or **6** (Figure AI.6) with cell membranes provided a detectable Cy5 emission; $Ir(ppy)_3$ emission remained quenched.

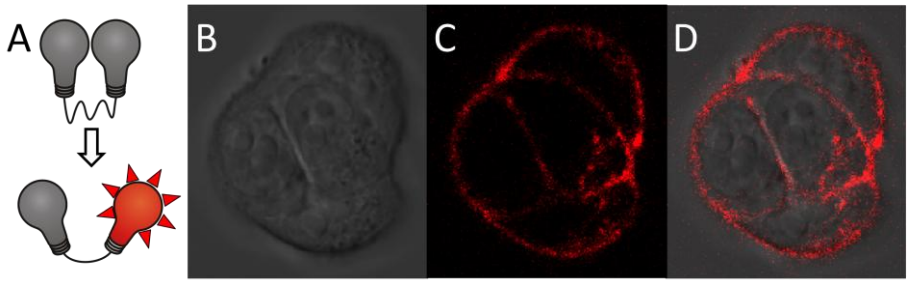

Figure 2: A) Schematic representation of partial activation by conformational change of the probe. B-D) Confocal microscope image of 4T1 cells after 1h incubation with 5 at 4 °C. B) Differential interference contrast, C) Cy5, D) overlay.

In **6**, the quenching of both $Ir(ppy)_3$ and Cy5 can be fully undone by cleavage of the connective bond between the two dyes (Figure 3A). To study the full activation, the disulfide bond of **6** (a model system for cleavage) was initially cleaved using cysteamine (Scheme AI.2). In MeOH:PBS 4:1, after 1h at RT, the cleavage reaction induced by an excess of cysteamine yielded an intensity increase of both $Ir(ppy)_3$ phosphorescence (100-fold increase, Figure 3C) and Cy5 fluorescence (a further 3-fold increase on the 30-fold increase caused by the solvent, making a total 90-fold, Figure 3D). In PBS a 200-fold increase of Cy5 fluorescence intensity was observed (Figure AI.7). After cleavage the end

products were analyzed using HPLC and mass spectrometry (Figures AI.8 and AI.9).

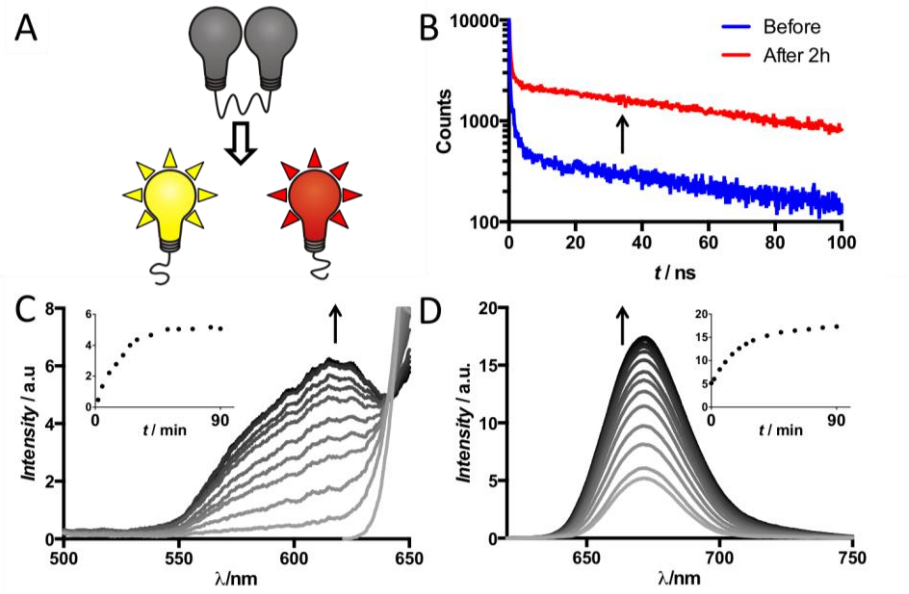

Figure 3: A) Schematic representation of disulfide cleavage, B) difference in luminescence decay before and after cleavage in solution, C) increase of luminescence of $Ir(ppy)_3$ and D) Cy5 upon cleavage. Insets in C) and D) are the change of peak height over time.

In vitro evaluation of the disulfide bond cleavage was performed in the 4T1 murine breast tumor cell line. After passive cellular internalization at 37 °C, Ir-S-S-Cy5 (**6**) was confined in the lysosomes of the cell, where the disulfide bond was reduced by a redox enzyme or an intracellular thiol.[29] We observed activation of both $Ir(ppy)_3$ and Cy5 in the lysosomes (Figure 4; Figure AI.10) and even when a high concentration (5 µM) of **6** surrounded the cells, only the cleaved components were visible (Figure AI.11). No $Ir(ppy)_3$ signal activation was observed when cells were incubated at 37 °C with **5** (Figure AI.12).

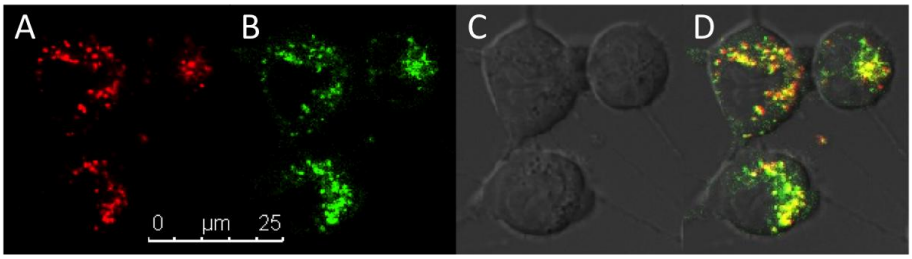

Figure 4: Confocal microscope images of 4T1 cells after 24h incubation with 6 at 37 °C. A) Cy5 in red, B) Ir(ppy)$_3$ in green, C) differential interference contrast, D) overlay of all channels. Yellow indicates overlay of red and green.

Luminescence lifetime measurements showed minor differences between the iridium complexes **1**, **2**, and **3** (Table 1). Conjugation with Cy5 (**4**) drastically shortened the lifetime. A short-lived species (τ < 1 ns), representative for residual Cy5 emission, accounted for a large part of the total emission at 600 nm; 89 % in **5** and 91 % in **6** (Figure AI.13). After cleavage, there is a relative large increase of long-lifetime emission (Figure 3B), indicating re-activation of Ir(ppy)$_3$ phosphorescence. Activation effects observed in solution were confirmed *in vitro* by fluorescence lifetime imaging microscopy (FLIM) using two different cell lines, 4T1 and U2OS. Results were independent of cell type (Figures 5 and AI.14). With **5** (uncleavable), the lifetime was short, while after activation of **6** (cleavable) the lifetime increased to 90 ns, similar to control experiments (Figure AI.14A). The change in lifetime seen with FLIM provides a clear measure of the *in vitro* activation. Unfortunately, the suboptimal filter cube also allows for some background, giving an average in lifetime signal. A time-gated approach, which was not possible in our set-up, might prevent this.

Table 1: Luminescence lifetimes of selected compounds in MeOH:PBS 4:1

Compound	**1**	**2**	**3**	**4**[a]	**5**	**6**
τ fast (ns)	N.A.[b]	N.A.[b]	N.A.[b]	1.0	0.55 (89 %)[c]	0.35 (95 %)[c]
τ slow (ns)	97.2	79.4	87.5	N.A.[b]	78.6	91.1
Average τ (ns)	97.2	79.4	87.5	1.0	9.1	4.9

[A] Emission measured at 680nm [B] Not applicable [C] Relative signal contribution

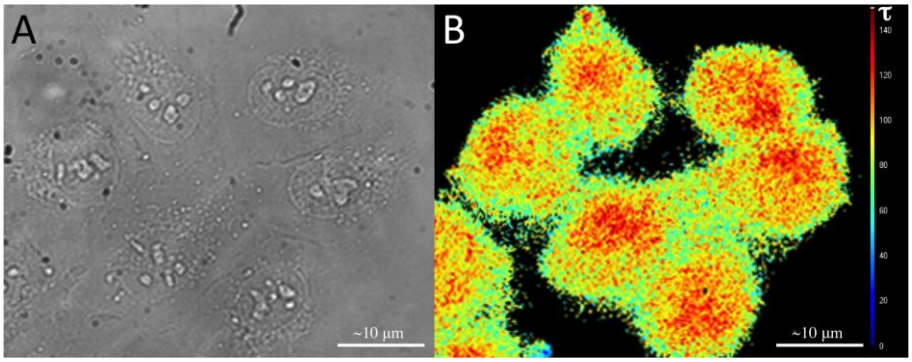

Figure 5: Fluorescence lifetime microscopy images of U2OS cells after 24h incubation with 6 at 37 °C using a CFP/YFP filter cube (excitation 436/12 & 500/20, dichroic 445 & 515, emission 467/37 & 545/45). A) Transmission, B) lifetime, the scale of the lifetimes is depicted on the right side (0-150 ns).

The lifetime technology proves to be a promising tool to analyze variations in cellular function related to disease progression.[10, 30] Although the here-described disulfide cleavage procedure is not specific, as every cell is able to cleave disulfide bonds,[29] it acts as a model system. In the future, derived activatable lifetime agents can in theory be used to detect expression levels of disease-related enzymes. When more disease-specific probes for FLIM are available, the scope of lifetime imaging may be expanded from *in vitro* to *in vivo* applications and maybe even to applications in image guided surgery.[31]

2.3. Conclusions

To conclude, the photophysical interactions between Cy5 and $Ir(ppy)_3$ were studied and used to generate an unprecedented activatable (long) lifetime imaging agent (**6**). The Cy5 emission of this agent depends on the polarity of the environment, while both the Cy5 and $Ir(ppy)_3$ emission can be activated by cleavage of the connective bond. In our view activatable long lifetime imaging agents provide a promising tool for future molecular imaging related to disease progression, complementary to intensity-based fluorescence detection.

1. Chin, P.T.K., et al., Optical imaging as an expansion of nuclear medicine: Cerenkov-based luminescence vs fluorescence-based luminescence. Eur J Nucl Med Mol I, 2013. 40(8): p. 1283-1291.
2. Weissleder, R. and V. Ntziachristos, Shedding light onto live molecular targets. Nat Med, 2003. 9(1): p. 123-128.
3. Urano, Y., Novel live imaging techniques of cellular functions and in vivo tumors based on precise design of small molecule-based 'Activatable' fluorescence probes. Curr Opin Chem Biol, 2012. 16(5-6): p. 602-608.
4. Lovell, J.F. and G. Zheng, Activatable smart probes for molecular optical imaging and therapy. J Innov Opt Heal Sci, 2008. 1(1): p. 45-61.
5. Huang, C.W., Z.B. Li, and P.S. Conti, Radioactive Smart Probe for Potential Corrected Matrix Metalloproteinase Imaging. Bioconjugate Chem, 2012. 23(11): p. 2159-2167.
6. Tung, C.H., et al., In vivo imaging of proteolytic enzyme activity using a novel molecular reporter. Cancer Res, 2000. 60(17): p. 4953-4958.
7. Urano, Y., et al., Rapid Cancer Detection by Topically Spraying a gamma-Glutamyltranspeptidase-Activated Fluorescent Probe. Sci Transl Med, 2011. 3(110): p. 110ra119.
8. Zhang, G., et al., Near-Infrared-Emitting Iridium(III) Complexes as Phosphorescent Dyes for Live Cell Imaging. Organometallics, 2014. 33(1): p. 61-68.
9. Alford, R., et al., Fluorescence lifetime imaging of activatable target specific molecular probes. Contrast Media Mol I, 2010. 5(1): p. 1-8.
10. Berezin, M.Y. and S. Achilefu, Fluorescence Lifetime Measurements and Biological Imaging. Chem Rev, 2010. 110(5): p. 2641-2684.
11. Ruggi, A., et al., Dendritic Ruthenium(II)-Based Dyes Tuneable for Diagnostic or Therapeutic Applications. Chem-Eur J, 2011. 17(2): p. 464-467.
12. Steunenberg, P., et al., Phosphorescence Imaging of Living Cells with Amino Acid-Functionalized Tris(2-phenylpyridine)iridium(III) Complexes. Inorg Chem, 2012. 51(4): p. 2105-2114.

13. Murphy, L., et al., The time domain in co-stained cell imaging: time-resolved emission imaging microscopy using a protonatable luminescent iridium complex. Chem Commun, 2010. 46(46): p. 8743-8745.
14. Xiong, L., et al., Phosphorescence Imaging of Homocysteine and Cysteine in Living Cells Based on a Cationic Ir (III) Complex. Inorg Chem, 2010. 49(14): p. 6402-6408.
15. Li, G., et al., Thiol-specific phosphorescent imaging in living cells with an azobis(2,2'-bipyridine)-bridged dinuclear iridium(III) complex. Chem Commun, 2013. 49(20): p. 2040-2042.
16. Ruggi, A., F.W.B. van Leeuwen, and A.H. Velders, Interaction of dioxygen with the electronic excited state of Ir(III) and Ru(II) complexes: Principles and biomedical applications. Coordin Chem Rev, 2011. 255(21-22): p. 2542-2554.
17. Zhong, W., P. Urayama, and M.A. Mycek, Imaging fluorescence lifetime modulation of a ruthenium-based dye in living cells: the potential for oxygen sensing. J Phys D Appl Phys, 2003. 36(14): p. 1689-1695.
18. Baggaley, E., et al., Dinuclear Ruthenium(II) Complexes as Two-Photon, Time-Resolved Emission Microscopy Probes for Cellular DNA. Angew Chem Int Ed Engl, 2014. 53: p. 3367-3371.
19. Shiu, H.Y., M.K. Wong, and C.M. Che, "Turn-on" FRET-based luminescent iridium(III) probes for the detection of cysteine and homocysteine. Chem Commun, 2011. 47(15): p. 4367-4369.
20. Costa, R.D., et al., A Deep-Red-Emitting Perylenediimide-Iridium-Complex Dyad: Following the Photophysical Deactivation Pathways. J Phys Chem C, 2009. 113(44): p. 19292-19297.
21. Rachford, A.A., et al., Boron Dipyrromethene (Bodipy) Phosphorescence Revealed in Ir(ppy)(2)(bpy-C C-Bodipy) (+). Inorg Chem, 2010. 49(8): p. 3730-3736.
22. Jares-Erijman, E.A. and T.M. Jovin, FRET imaging. Nat Biotechnol, 2003. 21(11): p. 1387-1395.
23. Rae, M., A. Fedorov, and M.N. Berberan-Santos, Fluorescence quenching with exponential distance dependence: Application to the external heavy-atom effect. J Chem Phys, 2003. 119(4): p. 2223-2231.
24. Rothe, C., S. King, and A. Monkman, Long-range resonantly enhanced triplet formation in luminescent polymers doped with iridium complexes. Nat Mater, 2006. 5(6): p. 463-466.
25. Kuil, J., et al., Peptide-Functionalized Luminescent Iridium Complexes for Lifetime Imaging of CXCR4 Expression. Chembiochem, 2011. 12(12): p. 1896-1902.
26. Horvath, G., et al., Selecting the right fluorophores and flow cytometer for fluorescence resonance energy transfer measurements. Cytom Part A, 2005. 65A(2): p. 148-157.
27. Huang, Z.X., et al., Direct observation of delayed fluorescence from a remarkable back-isomerization in Cy5. J Am Chem Soc, 2005. 127(22): p. 8064-8066.
28. Williams, R.J., J.N. Phillips, and K.J. Mysels, The critical micelle concentration of sodium lauryl sulphate at 25-degrees-C. T Faraday Soc, 1955. 51(5): p. 728-737.
29. Saito, G., J.A. Swanson, and K.D. Lee, Drug delivery strategy utilizing conjugation via reversible disulfide linkages: role and site of cellular reducing activities. Adv Drug Deliv Rev, 2003. 55(2): p. 199-215.
30. Becker, W., Fluorescence lifetime imaging - techniques and applications. J Microsc-Oxford, 2012. 247(2): p. 119-136.
31. Sun, Y., et al., Endoscopic Fluorescence Lifetime Imaging for In Vivo Intraoperative Diagnosis of Oral Carcinoma. Microsc Microanal, 2013. 19(4): p. 791-798.